

The maximum density droplet to lower density droplet transition in quantum dots

A. D. Güçlü

Theory Center, Cornell University, Ithaca, NY 14853

C. J. Umrigar

Theory Center and Laboratory of Atomic and Solid State Physics, Cornell University, Ithaca, NY 14853

(Dated: June 17, 2021)

We show that, Landau level mixing in two-dimensional quantum dot wave functions can be taken into account very effectively by multiplying the exact lowest Landau level wave functions by a Jastrow factor which is optimized by variance minimization. The comparison between exact diagonalization and fixed phase diffusion Monte Carlo results suggests that the phase of the many-body wave functions are not affected much by Landau level mixing. We apply these wave functions to study the transition from the maximum density droplet state (incipient integer quantum Hall state with angular momentum $L = N(N-1)/2$) to lower density droplet states ($L > N(N-1)/2$).

I. INTRODUCTION

Advances in miniaturization and processing techniques of semiconductor systems have made it possible to create nanostructures containing only a small number of electrons [1, 2, 3, 4, 5, 6]. These quantum dots, also called artificial atoms, provide a crucial testing ground for many important quantum effects in low-dimensional systems. The system parameters can be tuned by controlling the dot geometry, electrostatic gate voltage, and by applying a magnetic field.

Experimental techniques such as capacitance spectroscopy [3, 4] or gated transport spectroscopy [5, 6] allow experimentalists to precisely control the number of electrons in a two-dimensional parabolic confining potential, and map their electronic properties as a function of the magnetic field. Such systems offer very rich quantum many-body effects, providing a link between two different branches of physics: In the limit of zero magnetic field the system acts like an atom, i.e., it exhibits shell structure and obeys Hund's first rule. On the other hand, for relatively modest magnetic fields the system exhibits incipient quantum Hall physics. A large number of transitions induced by the magnetic field can be observed experimentally. The transitions can be understood from Hartree-Fock theory or from density functional theory (at low magnetic fields even the simple constant interaction model [7] suffices) but at high magnetic fields an accurate treatment of many-body effects is important.

The aim of this work is to study in detail the transitions between many-body states for moderately large magnetic field values where the angular momentum of the system increases beyond that of the so called maximum density droplet (MDD) regime [6], corresponding to the filling factor $\nu = 1$ in quantum Hall physics. Most of the previous work on the transition between MDD to lower density states (LDD) was performed in the lowest Landau level (LLL) approximation and/or was restricted to spin polarized electrons [8, 9, 10, 11, 12, 13]. The LDD states are not always predicted to be fully spin polarized, both in the absence of Landau level (LL) mixing [8] and

in the presence of LL mixing [14].

Here, we combine exact diagonalization and quantum Monte Carlo (QMC) techniques [15, 16, 17] to obtain a very accurate description of many-body states beyond the MDD. Linear combinations of determinants obtained by exact diagonalization within the LLL approximation serve as the starting point for building trial wave functions for our variational Monte Carlo (VMC) and diffusion Monte Carlo (DMC) calculations. The method described here is very systematic, can be applied to any eigenstate, and, is more efficient than exact diagonalization with LL mixing. Trial wave functions obtained by the exact diagonalization method have the right symmetry properties, including conservation of total angular momentum L , total spin S , and separability of center of mass and relative motion, which allows us to study center of mass excitations [18]. We apply our method to investigate the many-body states involved in the MDD-LDD transition. We find that for the $N = 4$ electron system, the pair densities of the ground and excited states close to the MDD-LDD transition have a well defined square symmetry, while those for $N = 6$ states have little structure. We find that the MDD-LDD transition acts as a convergence point for special values of (L, S) which correspond to the magic numbers [19]. The redistribution of electronic charge is rather smooth in the absence of the Zeeman effect, but, when a Zeeman term is included in the Hamiltonian it becomes more abrupt.

II. MODEL AND METHOD

A. Hamiltonian

We consider an N -electron two-dimensional quantum dot with a circularly symmetric parabolic confinement potential. Within the effective mass approximation, and neglecting finite thickness effects, the Hamiltonian in an

external magnetic field, B , is

$$H = \sum_j^N \left(\frac{1}{2m^*} \left(\mathbf{p}_j + \frac{e}{c} \mathbf{A}(\mathbf{r}_j) \right)^2 + \frac{1}{2} m^* \omega_0^2 \mathbf{r}_j^2 \right. \\ \left. + \frac{e^2}{\epsilon} \sum_{i < j}^N \frac{1}{r_{ij}} + g^* \mu_B B s_{z,j} \right), \quad (1)$$

where m^* is the effective mass of electron, \mathbf{A} is the vector potential, ω_0 is the parameter characterizing the parabolic confinement potential, ϵ is the dielectric constant, g^* is the effective g -factor, μ_B is the Bohr magneton and $s_{z,j}$ is the z -component of the spin of the j^{th} electron.

We use standard materials constants corresponding to GaAs, $m^* = 0.067m_0$, dielectric constant $\epsilon = 12.4$ and $g^* = -0.44$. Results will be given in effective atomic units ($\hbar = e^2/\epsilon = c = m^* = 1$): the effective Bohr radius is $a_0^* = 9.79373$ nm, and the effective Hartree is $H^* = 11.8572$ meV. We choose the confinement parameter $\hbar\omega_0$ to be $0.28 H^*$ or 3.32 meV, which is within the typical experimental range [4, 5, 6].

B. Single-particle states

Ignoring the interaction term, the single particle Fock-Darwin energies of this Hamiltonian are [20]

$$\epsilon_{n_r l} = (2n_r + |l| + 1)\hbar\omega - \frac{l\hbar\omega_c}{2}, \quad (2)$$

where $\omega_c = eB/m^*c$ is the cyclotron frequency, $\omega = \sqrt{\omega_0^2 + \omega_c^2/4}$, n_r is the radial quantum number and l is the angular quantum number ($n_r, |l| = 0, 1, \dots, \infty$). Equivalently, the energy spectrum can be expressed as a sum of two harmonic-oscillators [9],

$$\epsilon_{nm} = (n + 1/2)\hbar\omega_+ + (m + 1/2)\hbar\omega_-, \quad (3)$$

where $\omega_{\pm} = \omega \pm \omega_c/2$, n is the Landau level index, $n, m = 0, 1, \dots, \infty$ and $l = -n, -n + 1, \dots, \infty$. The relationship between these two sets of quantum numbers is $l = m - n$, $n_r = \min(n, m)$ or $n = n_r + \frac{|l-l|}{2} = n_r + \max(0, -l)$, $m = n_r + \frac{|l+l|}{2} = n_r + \max(0, l)$.

At zero B the energies depend only on the principal quantum number, $2n_r + |l| = n + m$, whereas at infinite B they depend only on the Landau level index n . The corresponding eigenfunctions $|nm\sigma\rangle$ (σ is the spin index) are used as the basis set in our exact diagonalization and QMC calculations of interacting dots. At zero magnetic field the system has degeneracies and therefore a shell structure, as in the case of real atoms. When a magnetic field is applied, the degeneracy is broken and several transitions occur due to single-electron level crossings as described by Eq. 2. Eventually all the electrons are in lowest Landau level orbitals and each of these orbitals is doubly occupied. In a noninteracting electron

picture no more transitions are predicted as the magnetic field is increased further, but, experimentally they are observed [6]. These can be understood from Hartree-Fock or density functional theory. The intra Landau level splittings get smaller with increasing B and the exchange interaction favors parallel spins, leading to spin flips, until eventually all the spins are parallel and the N lowest angular momentum states are occupied singly. This is the maximum density droplet (MDD) state. As B is increased further, Hartree-Fock [21] and density functional calculations [22, 23] predict an edge reconstruction due to some electrons jumping from low angular momentum states to higher angular momentum states because the Coulomb interaction overwhelms the parabolic external potential. These lower density droplet (LDD) states were observed experimentally [24] but quantitative discrepancies with experiments exist. Since several determinants of LLL noninteracting orbitals are exactly degenerate it is expected that an accurate treatment of correlation is important. This is the range of B that we study in this paper.

C. Many-particle states and Exact diagonalization

The many-body wave functions may be chosen to be eigenstates of the total angular momentum $\hat{L} \equiv \hat{L}_z$, total spin \hat{S}^2 and the z -component of total spin \hat{S}_z . In addition, the dynamic symmetry of an isotropic parabolic potential leads to the separability of center of mass and relative motion and the existence of two *center of mass operators* [18], \hat{C}_+ and \hat{C}_- that commute with the \hat{H} , \hat{L} , \hat{S}^2 and \hat{S}_z , and the above operators:

$$\hat{C}_+ = \frac{1}{N} \sum_{n'm'\sigma'nm\sigma} \sqrt{(n'+1)n} \hat{c}_{(n'+1)m'\sigma'}^\dagger \hat{c}_{n'm'\sigma'} \hat{c}_{(n-1)m\sigma}^\dagger \hat{c}_{nm\sigma} \quad (4)$$

$$\hat{C}_- = \frac{1}{N} \sum_{n'm'\sigma'nm\sigma} \sqrt{(m'+1)m} \hat{c}_{n'(m'+1)\sigma'}^\dagger \hat{c}_{n'm'\sigma'} \hat{c}_{n(m-1)\sigma}^\dagger \hat{c}_{nm\sigma}. \quad (5)$$

Determinants of Fock-Darwin orbitals are eigenfunctions of \hat{L} and \hat{S}_z . Thus, the many-body Hamiltonian in a determinantal basis is block diagonal, with the blocks corresponding to different (L, S_z) values. Also, we note that LLL determinants are eigenfunctions of \hat{C}_+ with eigenvalues $C_+ = 0$. The size of the subspaces can be further reduced by employing linear combinations of determinants, known as configuration state functions (CSFs), that are eigenstates of \hat{S}^2 and \hat{C}_- . The diagonalization of \hat{S}^2 and \hat{C}_- is done as explained in Ref.(18). The matrix elements of the Coulomb interaction can be determined either by numerical integration or analytically [27, 28, 29].

For a state with a given total angular momentum L ,

and for a given number of Landau levels, n , only single-particle states with angular momentum $l_{\min} \leq l \leq l_{\max}$ contribute, where $l_{\min} = -n$. For fully spin polarized LLL wave functions, $l_{\max} = L - (N - 1)(N - 2)/2$ and for lower spin states it is higher than that. As the number of Landau levels is increased, l_{\max} increases, both because the remaining $N - 1$ electrons can lower their angular momenta by occupying more than one Landau level and because the n^{th} Landau level has states with $l \geq -n$. Empirically we find that determinants containing orbitals with $l > 2L/N + 1$ contribute little to the wave function and consequently we could limit ourselves to orbitals with $l \leq 2L/N + 1$. However, in most cases we avoid doing this because the wave functions are no longer exact eigenstates of the operator \hat{C}_- .

D. Quantum Monte Carlo

In this work, we use both the variational Monte Carlo (VMC) and the diffusion Monte Carlo (DMC) methods [15, 16, 17] to improve the exact diagonalization wave functions and energies obtained within the LLL. First, we introduce variational parameters by multiplying the LLL wave function by a Jastrow factor and optimize the Jastrow parameters by minimizing the variance of the local energy [30]. For a given state (L, S, S_z, C_-) , the form of our trial wave functions is

$$\Psi_T^{L,S,S_z,C_-} = J_{ee} J_{ed} J_{eed} \sum_i^{N_{\text{CSF}}} \alpha_i \Psi_D^{L,S,S_z,C_-}, \quad (6)$$

where J_{ee}, J_{ed}, J_{eed} are the electron-electron, electron-dot, and electron-electron-dot Jastrow terms respectively. The CSF's Ψ_D^{L,S,S_z,C_-} are obtained by diagonalizing the \hat{S}^2 and \hat{C}_- matrices. Multiplying by the Jastrow factor does not alter the L, S^2 and S_z symmetries of the wave function, aside from introducing a completely negligible amount of spin contamination [31] (not an exact eigenstate of \hat{S}^2), arising from the different cusp conditions for parallel- and antiparallel-spin electrons. The Jastrow factor reduces the statistical error in both VMC and DMC for a given number of Monte Carlo steps. It also lowers the VMC energy, but leave the fixed-phase DMC energy (described later) unchanged because the phase of the trial wave function is not altered.

The linear coefficients α_i are obtained by diagonalizing \hat{H} . They can also serve as additional free parameters that can be reoptimized in VMC. However, we have found that, at sufficiently large magnetic fields, there is no gain in energy from reoptimizing them, and the exact LLL wave function multiplied by the optimized Jastrow factor provides an excellent trial wave function. This is in contrast to the situation in the absence of a magnetic field, where the reoptimized linear coefficients in the presence of the Jastrow factor are considerably smaller in magnitude than the original ones from exact diagonalization. This can be understood as follows. Quan-

tum chemists distinguish between static correlation (also known as near-degeneracy correlation) and dynamic correlation. Within the quantum Monte Carlo literature it is well understood that static correlation is most effectively incorporated into the wave function by using a linear combination of nearly degenerate determinants, whereas dynamic correlation is most efficiently treated by a flexible Jastrow factor. In the case of dots in sufficiently large magnetic fields the separation of energy scales (intra Landau level versus inter Landau level) is very large and the distinction between static and dynamic correlation becomes sharp.

For any given state, the determinantal coefficients α_i , for a LLL wave function, need not be recalculated when the system parameters m^*, ω_0, B and ϵ are varied, because the α_i are independent of these system parameters. This is because all the LLL determinants with a given L have the same expectation value for the single-particle Hamiltonian. So the single-particle terms in the Hamiltonian contribute a multiple of the unit matrix and only the interaction part of the Hamiltonian need be diagonalized. Hence, the LLL wave function is independent of ϵ , and, depends on m^*, ω_0 and B only through a scaling of the linear dimensions by the factor $\sqrt{1/m^* \omega}$. Consequently these Jastrow-LLL wave functions are not only a very accurate choice but also a very efficient choice for QMC calculations. Of course this does not apply to low angular momentum L states because it is impossible to construct them using only LLL orbitals. Note also that the independence of the α_i on the system parameters makes the Fock-Darwin orbitals the most efficient choice, as opposed to using say Hartree Fock or density functional orbitals.

The DMC method improves upon the VMC energy by projecting onto the lowest energy wave function that has the same nodes (or the same phase in the case of complex wave functions) as the trial wave function. The resulting fixed-node or fixed-phase energies are upper bounds to the true energies and consequently the accuracy of the calculations depends on the quality of the nodes or the phase of the trial wave functions. We employ an efficient implementation of DMC described in Ref. 35. Since we use complex trial wave functions, we employ the fixed phase approximation [32], which has previously been applied to quantum dot systems [33, 34]: starting from a variational wave function Ψ_T , a new function $f = \Phi^* \Psi_T$ is introduced, where Φ is the ground state of the N -body Hamiltonian subject to the constraint that it have the same phase as Ψ_T . The integral form of the Schrödinger equation in imaginary time ($t \rightarrow it$) then can be written in terms of f as:

$$f(\mathbf{R}, t + \tau) = \int d\mathbf{R}' \tilde{G}(\mathbf{R}, \mathbf{R}', \tau) f(\mathbf{R}', t), \quad (7)$$

where \mathbf{R} represents the coordinates of N electrons, $G(\mathbf{R}, \mathbf{R}', \tau) = \Psi_T(\mathbf{R}) \langle \mathbf{R} | e^{-\tau \hat{H}} | \mathbf{R}' \rangle / \Psi_T(\mathbf{R}')$, is a Green function that is explicitly known only in the short-time limit ($\tau \rightarrow 0$). Hence, the Eq.(7) can be solved by apply-

ing G repeatedly until the desired projection is obtained. Since the function f is used as a probability density for Monte Carlo sampling, it must be real and positive which is equivalent to the assumption that the phase of Φ is the same as that of the trial wave function Ψ_T . After equilibration, the energy can be calculated as an average over the sampled points \mathbf{R}_m :

$$E \approx \frac{1}{M} \sum_m E_L(\mathbf{R}_m), \quad (8)$$

where E_L is the real part of the local energy,

$$E_L(\mathbf{R}) = \text{Re} \left\{ \Psi_T(\mathbf{R})^{-1} \hat{H} \Psi_T(\mathbf{R}) \right\}. \quad (9)$$

We note, however, that for an external potential with circular symmetry it is also possible to use the fixed node approximation: In the subspace of the good quantum number L , the Hamiltonian can be written as

$$\hat{H} = \sum_j \left(\frac{1}{2m^*} \mathbf{p}_j^2 + \frac{1}{2} m^* \omega^2 \mathbf{r}_j^2 + \frac{e^2}{\epsilon} \sum_{i \neq j} \frac{1}{r_{ij}} \right) - \frac{1}{2} \hbar \omega_c L \quad (10)$$

which is purely real. We can ignore the last term in \hat{H} since it just gives a trivial shift in the energies of the various L states. For the remaining part of \hat{H} , states with angular momentum L and $-L$ are degenerate and so we can consider their sum, which is real. It is possible to expand these real LLL wave functions in terms of real orbitals, but the number of determinants increases greatly. For instance, a MDD state can be written as a single determinant of complex orbitals or a sum of 2^{N-1} determinants of real orbitals. So, it is more efficient to use complex wave functions within the fixed phase approximation.

III. RESULTS AND DISCUSSION

We now apply the techniques described above to quantum dots similar to those studied experimentally [4, 5, 6], in magnetic fields ranging from 3 – 8 Tesla bringing the dots in the vicinity of MDD-LDD transition. Since the Zeeman term just results in a trivial shift of the different S_z states relative to each other, we will ignore the Zeeman term unless explicitly stated otherwise.

A. Comparison between Exact diagonalization and QMC

In this subsection, we compare results obtained from exact diagonalization and QMC calculations with different levels of approximation. Fig. 1 shows the energies of $N = 4$ and $N = 7$ fully spin polarized electrons at $B = 8$ T and $B = 5$ T respectively. The solid line represents the results obtained by exact diagonalization within

the LLL approximation, from which we build QMC trial wave functions. The dotted lines are the exact diagonalization results with 2 LLs included. The DMC results, using the Jastrow-LLL wave functions, are represented with the crosses. The numbers represent C_- , with 0 indicating that there is no center of mass excitation. As seen from Fig. 1, DMC energies are very accurate, better than those from a 2 LL diagonalization. This is particularly clear in Fig. 1(b) where the magnetic field is only 5 T since LL mixing is more important at lower magnetic fields. For 4 spin-polarized electrons there is no real computational advantage to using QMC over exact diagonalization, but, for spin unpolarized dots and/or higher numbers of electrons the QMC method becomes more efficient, because the number of determinants needed is dramatically smaller. For instance, in Fig. 1(b) the QMC calculation for $L = 29$ using 21 determinants in the trial wave function clearly gives a better energy than a 2 LL diagonalization using 28637 determinants. These results also verify the appearance of magic numbers, *i.e.* particular angular momenta, L^* , at which a deep dip occurs, followed by a center of mass excitation at $L^* + 1$ [1, 19]. Also, we note that for $N = 7$, within the LLL approximation exact diagonalization makes an incorrect prediction for the ground state which underscores the need to go beyond the LLL approximation near the MDD-LDD transition.

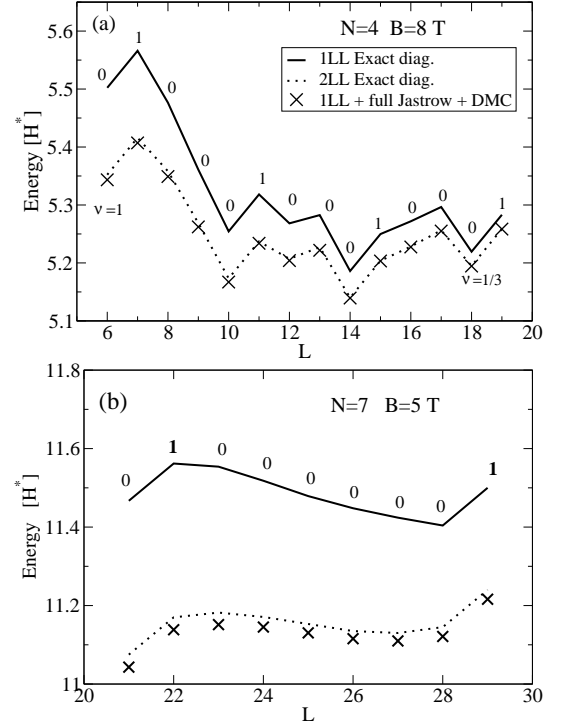


FIG. 1: Energy as a function of total angular momentum L , for (a) $N = 4$ at $B = 8$ T, (b) $N = 7$ at $B = 5$ T, obtained by exact diagonalization in LLL approximation (solid line), exact diagonalization including 2LLs (dotted line), and DMC using full Jastrow term (cross marks). The numbers above the line represent the C_- quantum number.

TABLE I: Comparison of energies for different L values ($N = 4$, $S = 2$, $B = 8$ T) obtained from exact diagonalization method within 1,2, and 3 LL approximations (ED), VMC including only the electron-electron part of the Jastrow factor (e-e VMC), and DMC using a fully optimized Jastrow factor (DMC). The energy differences between DMC and the 3-LL exact diagonalization, shown in the last column, are small, with the DMC energies being better in most cases.

L	1LL ED	2LL ED	3LL ED	e-e VMC	DMC	DMC-ED
6	5.5022	5.3522	5.3463	5.3459	5.3434	-29×10^{-4}
7	5.5660	5.4159	5.4100	5.4096	5.4071	-29×10^{-4}
8	5.4764	5.3582	5.3511	5.3517	5.3491	-20×10^{-4}
9	5.3609	5.2688	5.2641	5.2634	5.2622	-19×10^{-4}
10	5.2544	5.1733	5.1705	5.1738	5.1702	-3×10^{-4}
11	5.3182	5.2370	5.2343	5.2376	5.2339	-4×10^{-4}
12	5.2683	5.2070	5.2042	5.2064	5.2041	-1×10^{-4}
13	5.2825	5.2272	5.2227	5.2239	5.2218	-9×10^{-4}
14	5.1860	5.1401	5.1394	5.1417	5.1394	-0×10^{-4}
15	5.2498	5.2038	5.2031	5.2058	5.2033	2×10^{-4}
16	5.2718	5.2282	5.2272	5.2301	5.2275	3×10^{-4}
17	5.2965	5.2563	5.2548	5.2574	5.2550	2×10^{-4}
18	5.2194	5.1948	5.1946	5.1953	5.1946	0×10^{-4}
19	5.2831	5.2586	5.2583	5.2590	5.2584	1×10^{-4}

TABLE II: Same as table I but for $S = 0$ and $B = 5$ T.

L	1LL ED	2LL ED	3LL ED	e-e VMC	DMC	DMC-ED
6	4.7787	4.5007	4.4846	4.5041	4.4852	6×10^{-4}
7	4.7943	4.5479	4.5365	4.5512	4.5346	-9×10^{-4}
8	4.4924	4.3872	4.3833	4.3864	4.3825	-8×10^{-4}
9	4.5875	4.4824	4.4784	4.5075	4.4787	3×10^{-4}
10	4.4911	4.4150	4.4131	4.4175	4.4132	1×10^{-4}

The energies from 3 LL diagonalizations are indistinguishable from the DMC energies on the scale of the plots, so we present them as tables. In Table I we show the energies for $N = 4$, $S = 2$, $B = 8$ T and in Table II for $N = 4$, $S = 0$, $B = 5$ T. We have also included the results obtained by including only the electron-electron part of the Jastrow factor. The electron-electron Jastrow recovers most of the missing energy by keeping electrons apart, in agreement with the VMC calculations of spin polarized electrons in Ref. 36. For spin polarized electrons DMC gives better energies than 3 LL calculations especially for the lower L values. For higher L , electrons occupy larger orbits, making the electron-electron Jastrow less important. Thus, the effect of LL mixing is less important and exact diagonalization results agree with QMC results within a few standard deviations ($\approx 1 \times 10^{-4}$ H*) of the QMC results. For spin unpolarized electrons,

while the QMC results are not particularly superior to 3 LLs results, agreement still remains excellent as seen in Table II. Since both VMC and DMC calculations are performed within the fixed phase approximation, we conclude that exact LLL wave functions have very accurate phases.

B. MDD-LDD transition

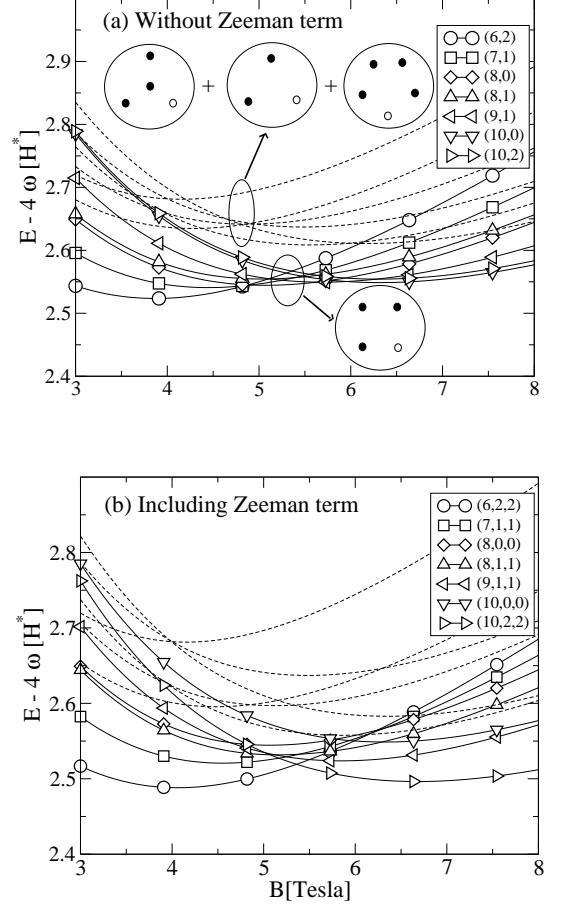


FIG. 2: Energy as a function of magnetic field for different many-body states for $N = 4$, (a) without Zeeman term, (b) with Zeeman term. Lines with symbols represent many-body states which are closely involved in the MDD-LDD transition, and they are identified by their (L, S) values in (a), and by their (L, S, S_z) values in (b). The locations of the maxima in the pair densities are indicated by solid dots, and, open dots represent the fixed electrons.

Having established the accuracy of the form of the wave function, in this subsection, we study in detail the MDD-LDD transition for $N = 4$ and $N = 6$. Fig. 2 shows the energies as a function of magnetic field for different many-body states (L, S) (S_z is also given in Fig. 2(b)) closely involved in MDD-LDD transition. In Fig. 2(a), the Zeeman splitting is not taken account, so the states are $2S + 1$ -fold degenerate. It should be noted that, in

these calculations only the states with angular momentum $N(N-1)/2 \leq L \leq N(N+1)/2$ are considered. For the fully spin polarized case the MDD-LDD transition involves only the $L = N(N-1)/2$ and $L = N(N+1)/2$ states [8, 19], but LLL exact diagonalization energies indicate that other angular momentum states between these values are expected to become ground states for spin unpolarized or partially polarized electrons [8]. The excitation spectrum in Fig. 2(a) reveals a very interesting structure, involving several many-body states in a small region near the MDD-LDD transition which occurs at $B \approx 5.5$ T: While these states (shown by solid lines with symbols) don't seem to have a regular predictable (L, S) pattern, they correspond to the magic number sequences of different S states for $N = 4$ [19, 25, 26]. Strikingly, the MDD-LDD transition acts as a convergence point for these particular (L^*, S^*) values. On the other hand, when the Zeeman effect is taken into account (we consider an effective Landé factor $g^* = -0.44$), higher spin states are favored and the separation between the solid lines with symbols and dashed lines become less clear.

An interesting property of these states can be revealed by plotting their pair-density $\rho(\mathbf{r}_1, \mathbf{r}_2)$ (probability density of two electrons being at \mathbf{r}_1 and \mathbf{r}_2), with the reference electron \mathbf{r}_2 fixed at a density maximum. As schematically shown in Fig. 2(a), the lower energy states all have the same structure, with electrons arranged in a square. In fact, square symmetry corresponds to the minimum energy electronic arrangement of classical point charges [19]. The higher energy states (dashed lines) have their electrons arranged in a centered triangle, except for the two center of mass excited states $(L, S, C_-) = (7, 2, 1)$ and $(9, 0, 1)$. These two states show 3 and 5 peaks respectively in their pair-densities instead of the more intuitive 4-peak structure (including the reference electron) one would expect for a $N = 4$ dot. We have also observed similar structures in other center of mass excitations for higher L values.

In Fig. 3 we study the ground state pair densities at magnetic fields between 5 – 6 T as the system goes from the MDD state to the LDD states. Without Zeeman splitting, there is a smooth electronic redistribution involving the states $(6, 2)$, $(8, 0)$, $(9, 1)$, and $(10, 0)$. with increased localization of electrons. Note that, in this case, the state $(10, 2)$ never becomes the ground state in agreement with the results of Ref.(18). When the Zeeman term is included, low spin states are suppressed and the system becomes fully polarized. As a result, the MDD-LDD transition is much more abrupt, going directly from the state $(6, 2)$ to the state $(10, 2)$. An abrupt charge redistribution in post-MDD transitions was observed experimentally also [6]. The dominant determinant in the $(10, 2)$ state has LLL orbitals with $l = 1, 2, \dots, N$ and consequently the density at the center of the dot is small.

In Fig. 4, we plot the energy spectrum for $N = 6$. As in the $N = 4$ case, we can distinguish between two sets of eigenstates when the Zeeman term is neglected (Fig.4(a)). We have only labeled the states that are

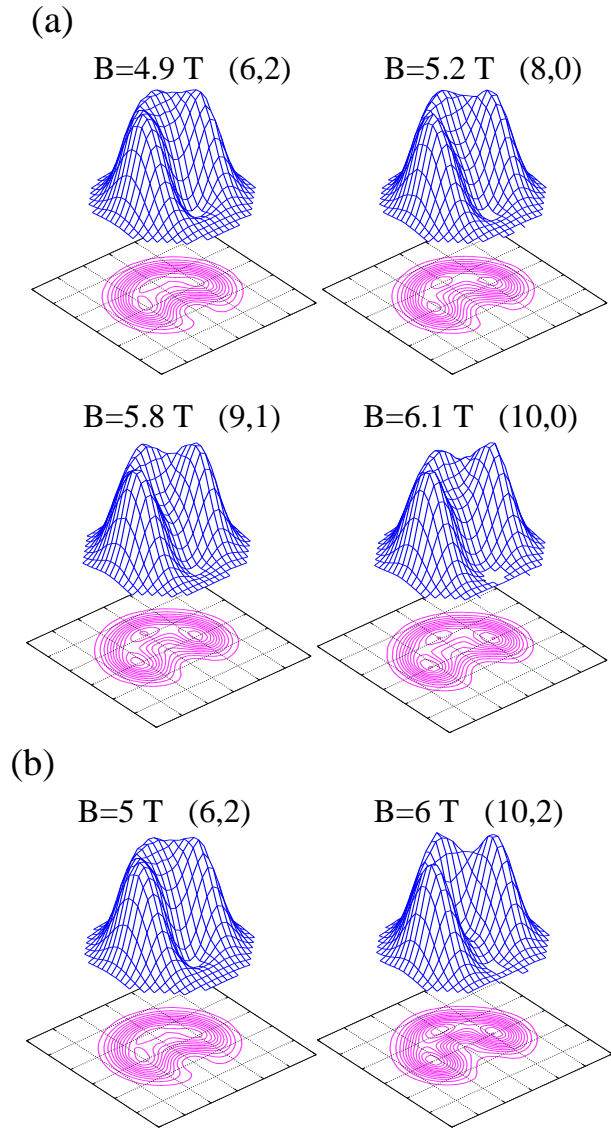


FIG. 3: (color online) Evolution of VMC ground state pair densities as a function of magnetic field for $N = 4$. (a) Without Zeeman effect (b) Including Zeeman effect.

closely involved in the MDD-LDD transition, marked by symbols. However, unlike the $N = 4$ case, we have found that, at the confinement strength considered here ($\omega_0 = 3.32$ meV), the pair densities of $N = 6$ dots near MDD-LDD transition have little structure (except for the $(21, 3)$ state which has a small hexagonal-shaped ripple). In Fig. 5, we plot the radial densities of the ground states that participate in the MDD-LDD transition, namely, $(15, 3)$, $(18, 0)$, $(19, 1)$, and $(21, 1)$. These ground state transitions are in agreement with those of Ref. 14 except for the last transition where they observe a large region where the $(20, 2)$ state occurs, followed by $(21, 3)$. In our calculations, as seen in Fig. 4, the $(21, 3)$ state occurs only if a Zeeman term is included. As a result of the Zeeman splitting, the charge redistribution during the

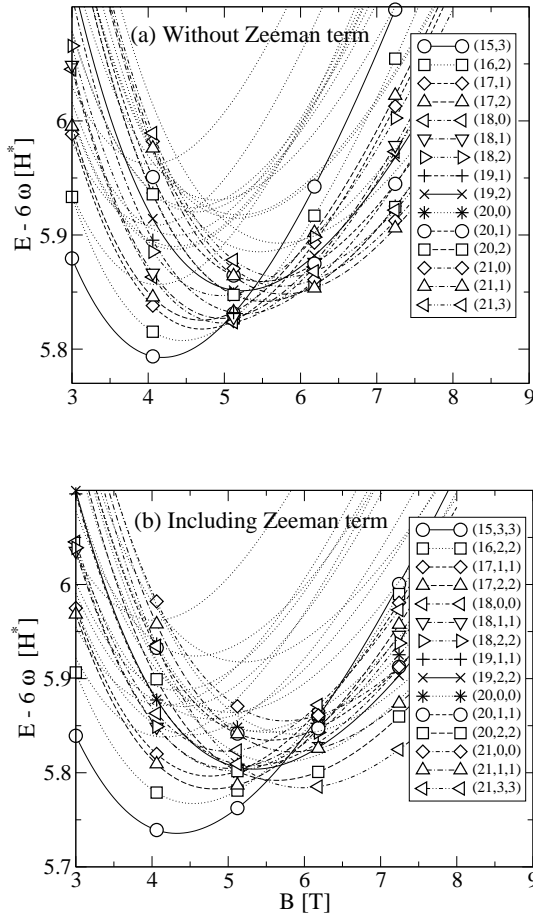


FIG. 4: Energy as a function of magnetic field for different many-body states for $N = 6$, (a) without Zeeman term, (b) with Zeeman term. Lines with symbols represent many-body states which are closely involved in the MDD-LDD transition, and they are identified by their (L, S) values in (a), and by their (L, S, S_z) values in (b).

MDD-LDD transition becomes more abrupt, as in the $N = 4$ dot.

IV. CONCLUSIONS

To summarize, by combining exact diagonalization and QMC methods, we have obtained highly accurate many-body wave functions and energies for circular parabolic dots in the range of magnetic fields corresponding to the MDD-LDD transition. In this regime, the dot goes through several angular momentum and spin transitions, and one does not expect Hartree-Fock theory, or, density functional theory with an approximate functional, to provide an accurate description. Exact diagonalization is prohibitively expensive because of the importance of Landau level mixing. Exact diagonalization wave functions within the LLL approximation are not sufficiently accurate on their own, but when they are multiplied by an optimized Jastrow and used as trial wave functions

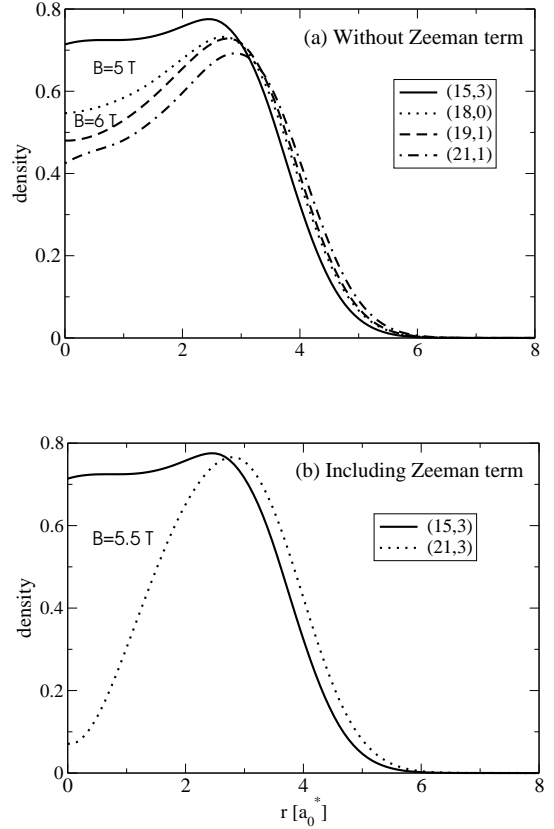


FIG. 5: Evolution of the ground state densities as a functions of magnetic field is increased for $N = 6$, obtained by VMC method. (a) Without Zeeman effect (b) Including Zeeman effect.

in DMC, they lead to very accurate energies. The high accuracy of the fixed phase DMC energies shows that the phase of exact wave functions is not strongly affected by LL mixing. The method described is very efficient since the trial wave functions have determinantal coefficients that are independent of system parameters m^* , ω_0 , B and ϵ , and the Jastrow optimization process is very fast and stable. We have found that near the MDD-LDD transition, the pair densities for $N = 4$ have a well defined square structure, whereas those for $N = 6$ have little structure. When the Zeeman energy is included, the next ground state beyond the MDD state is fully polarized and has $L = N(N+1)/2$. This leads to an abrupt redistribution of charge, as observed experimentally [6]. If instead the Zeeman energy is zero then several unpolarized and partially polarized states become ground states over a rather small range of magnetic fields and the charge redistribution is smaller and smoother. This could be verified experimentally. For instance, if a material for which the g -factor can be tuned to a small value is used, then the transition from unpolarized or partially polarized LDD states to fully polarized ones could be induced by increasing the effective g -factor by using tilted magnetic fields [37].

The number of electrons that can be studied with this

method is limited by the number of Slater determinants in the LLL approximation. This increases rapidly as the angular momentum increases beyond the MDD value, $L = N(N - 1)/2$. If the system is fully spin polarized, the number of determinants in the LLL approximation is much reduced and N can be much larger. When L is sufficiently large that the number of determinants in even the LLL becomes too large it is possible to dramatically reduce the number of determinants by employing composite fermion wave functions [38], which are very good approximations to the exact LLL wave functions. Once

again Landau level mixing can be incorporated very efficiently with QMC. This has been done for a 15-electron dot in Ref. 39.

V. ACKNOWLEDGMENTS:

We thank W. Geist, J. Jain, M. Korkusinski and F. Pederiva for helpful discussions. This work was supported by the NSF and FCAR.

-
- [1] *Quantum dots*, L. Jacak, P. Hawrylak, and A. Wojs, (Springer-Verlag Berlin, 1992).
 - [2] R.C. Ashoori, *Nature* (London) **379**, 413 (1996).
 - [3] R.C. Ashoori, H.L. Stormer, J.S. Weiner, L.N. Pfeiffer, S. J. Pearton, K.W. Baldwin, and K.W. West, *Phys. Rev. Lett.* **68**, 3088 (1992).
 - [4] R.C. Ashoori, H.L. Stormer, J.S. Weiner, L.N. Pfeiffer, K.W. Baldwin, and K.W. West, *Phys. Rev. Lett.* **71**, 613 (1993).
 - [5] L. P. Kouwenhoven, T. H. Oosterkamp, M. W. S. Danoe-sastro, M. Eto, D. G. Austing, T. Honda, and S. Tarucha, *Science* **278**, 1788 (1997).
 - [6] T.H. Oosterkamp, J.W. Janssen, L.P. Kouwenhoven, D. G. Austing, T. Honda, and S. Tarucha, *Phys. Rev. Lett.* **82**, 2931 (1999).
 - [7] P. L. McEuen, E. B. Foxman, J. Kinaret, U. Meirav, M. A. Kastner, N. S. Wingreen and S. J. Wind, *Phys. Rev. B* **45**, R11419 (1992).
 - [8] S.R.Eric Yang, A.H. MacDonald, and M.D. Johnson, *Phys. Rev. Lett.* **71**, 3194 (1993).
 - [9] P. Hawrylak, *Phys. Rev. Lett.* **71**, 3347 (1993).
 - [10] L. Martin-Moreno, J.J. Palacios, J.H. Oaknin, and C. Tejedor, *Physica B* **212**, 224 (1995).
 - [11] A. Wojs, and P. Hawrylak, *Phys. Rev. B* **56**, 13227 (1997).
 - [12] E. Goldmann and S.R. Renn, *Phys. Rev. B* **60**, 16611 (1999).
 - [13] M. Manninen, S. Viefers, M. Koskinen, S. M. Reimann, *Phys. Rev. B* **64**, 245322 (2001).
 - [14] S. Siljamaki, A. Harju, R. M. Nieminen, V. A. Sverdlov, and P. Hyvonen, *Phys. Rev. B* **65**, 121306(R) (2002).
 - [15] W. M. C. Foulkes, L. Mitas, R. J. Needs, and G. Rajagopal, *Rev. Mod. Phys.* **73**, 33 (2001).
 - [16] *Quantum Monte Carlo Methods in Physics and Chemistry*, edited by M. P. Nightingale and C. J. Umrigar, [NATO ASI Ser. C. **525** 101, 1999].
 - [17] B.L. Hammond, W.A. Lester and P.J. Reynolds, *Monte Carlo Methods in Ab Initio Quantum Chemistry*, (World Scientific 1994).
 - [18] A. Wensauer, M. Korkusinski, and P. Hawrylak, *Solid State Comm.* **130**, 115 (2004).
 - [19] P.A. Maksym, H. Imamura, G.P. Mallon, and H. Aoki, *J.Phys.: Condens. Matter* **12**, R299 (2000).
 - [20] V. Fock, *Z. Phys.* **47**, 446 (1928); C.G. Darwin, *Proc. Cambridge Philos. Soc.* **27**, 86 (1930).
 - [21] C. de C. Chamon and X. G. Wen, *Phys. Rev. B* **49**, 8227 (1994).
 - [22] M. Ferconi and G. Vignale, *Phys. Rev. B* **50**, 14722 (1994).
 - [23] M. Ferconi and G. Vignale, *Phys. Rev. B* **56**, 12108 (1997).
 - [24] O. Klein, C. de C. Chamon, D. Tang, D. M. Abusch-Magder, U. Meirav, X.-G. Wen, and M. A. Kastner, *Phys. Rev. Lett.* **74**, 785 (1995).
 - [25] R. K. Kamilla and J. K. Jain, *Phys. Rev. B* **52**, 2789 (1995).
 - [26] J. K. Jain and T. Kawamura, *Europhys. Lett.* **29**, 321 (1995).
 - [27] P. Hawrylak, *Solid State Commun.* **88**, 475 (1993).
 - [28] A. Wojs and P. Hawrylak, *Phys. Rev. B* **51**, 10880 (1995).
 - [29] E.V. Tsiper *J.Math.Phys* **43** 1664 (2002)
 - [30] C.J. Umrigar, K.G. Wilson, and J.W. Wilkins, *Phys. Rev. Lett.* **60**, 1719 (1988).
 - [31] C. J. Huang, C. Filippi and C. J. Umrigar, *J. Chem. Phys.* **108**, 8838 (1998).
 - [32] G. Ortiz, D. M. Ceperley, and R. M. Martin, *Phys. Rev. Lett.* **71**, 2777 (1993).
 - [33] F. Bolton, *Phys. Rev. B* **54**, 4780 (1996).
 - [34] A.D. Güçlü, J.S. Wang, and H. Guo, *Phys. Rev. B* **68**, 35304 (2003).
 - [35] C. J. Umrigar, M. P. Nightingale, and K. J. Runge, *J. Chem. Phys.* **99**, 2865 (1993).
 - [36] A. Harju, S. Siljamaki, and R. M. Nieminen, *Phys. Rev. B* **60**, 1807 (1999).
 - [37] J. Weis, R. J. Haug, K. v. Klitzing, and K. Ploog, *Phys. Rev. Lett.* **71**, 4019 (1993).
 - [38] G. S. Jeon, C.-C. Chang, and J. K. Jain *Phys. Rev. B* **69**, 241304(R) (2004).
 - [39] A. D. Güçlü, G. S. Jeon, C. J. Umrigar and J. K. Jain, to be submitted for publication.